PHOTONICS Research

Modulation properties of solitary and optically injected phased-array semiconductor lasers

Nianqiang Li,[1,*] H. Susanto,[2] B. R. Cemlyn,[1] I. D. Henning,[1] and M. J. Adams[1]

[1]School of Computer Science and Electronic Engineering, University of Essex, Wivenhoe Park, Colchester CO4 3SQ, UK
[2]Department of Mathematical Sciences, University of Essex, Wivenhoe Park, Colchester CO4 3SQ, UK
*Corresponding author: wan_103301@163.com

Received 12 April 2018; revised 9 July 2018; accepted 17 July 2018; posted 17 July 2018 (Doc. ID 328119); published 23 August 2018

We study modulation properties of two-element phased-array semiconductor lasers that can be described by coupled mode theory. We consider four different waveguide structures and modulate the array either in phase or out of phase within the phase-locked regions, guided by stability diagrams obtained from direct numerical simulations. Specifically, we find that out-of-phase modulation allows for bandwidth enhancement if the waveguide structure is properly chosen; for example, for a combination of index antiguiding and gain-guiding, the achievable modulation bandwidth in the case of out-of-phase modulation could be much higher than the one when they are modulated in phase. Proper array design of the coupling, controllable in terms of the laser separation and the frequency offset between the two lasers, is shown to be beneficial to slightly improve the bandwidth but not the resonance frequency, while the inclusion of the frequency offset leads to the appearance of double peak response curves. For comparison, we explore the case of modulating only one element of the phased array and find that double peak response curves are found. To improve the resonance frequency and the modulation bandwidth, we introduce simultaneous external injection into the phased array and modulate the phased array or its master light within the injection locking region. We observe a significant improvement of the modulation properties, and in some cases, by modulating the amplitude of the master light before injection, the resulting 3 dB bandwidths could be enhanced up to 160 GHz. Such a record bandwidth for phased-array modulation could pave the way for various applications, notably optical communications that require high-speed integrated photonic devices.

OCIS codes: (060.4080) Modulation; (140.5960) Semiconductor lasers; (140.3290) Laser arrays; (230.7400) Waveguides, slab.
https://doi.org/10.1364/PRJ.6.000908

1. INTRODUCTION

The properties of different directly modulated semiconductor laser structures are of considerable interest both in terms of their fundamental limits and for their potential use in a wide range of applications [1–10]. Conventionally modulation bandwidths are related to the frequency of relaxation oscillation of semiconductor lasers (typically several gigahertz) determined by the slow carrier–photon interaction. One approach to overcoming this has involved the use of optical injection locking, and this has been shown to lead to significantly increased modulation bandwidth [11,12]. This technique has been applied to conventional semiconductor lasers [13–17], semiconductor ring lasers [18], vertical-cavity surface-emitting lasers (VCSELs) [19,20], quantum dot/dash lasers [21], and quantum cascade lasers [22]. An alternative to injection locking involves the use of coupled laser systems, and these also have proved effective for enhancing modulation limits via the relatively fast photon–photon resonance effect [23–27]. In this paper we investigate coupled laser systems and focus on the modulation properties of a phased array consisting of two semiconductor lasers that are coupled via evanescent fields.

Studies of phased-array semiconductor lasers based on a range of structures have focused on various aspects, including high-power output [28,29], stability [30–33], gain tuning and parity-time symmetry breaking [34], turbulent chimeras [35], phase-locked state asymmetry related to gain and loss in two lasers [36], richness of dynamics [37–42], and a periodicity behavior with laser separation [43]. It is known that these devices are intrinsically unstable under certain conditions and can even develop complicated chaotic oscillations [44]. To enhance stability, the injection locking technique has also been applied to phased arrays, where only one or all elements are subject to external injection [45–47]. Interesting locking mechanisms and the influence of waveguiding parameters on locking regions

have been revealed [48,49]. In addition to the continuous wave (CW) operation, several groups have published notable results on the direct modulation of phased arrays. Fryslie *et al.* have reported numerically and experimentally the modulation of coherently coupled two-element photonic crystal VCSEL arrays, with modulation bandwidths greater than 30 GHz and up to 37 GHz [25]. Xiao *et al.* have experimentally demonstrated modulation bandwidth enhancement using coupled twin-square microcavity lasers, which showed good agreement with a rate equation analysis [26]. Wilson *et al.* have carried out a small signal analysis of the modulation response of phased-array semiconductor lasers at K-band frequencies and identified some design issues [27]. While much of this attention has focused upon the modulation properties of specific examples, here we focus on two specific aspects aiming at providing a better understanding of modulation of phased-array semiconductor lasers.

First, we examine the effects of basic design parameters in terms of waveguide structures, the laser separation, and the frequency offset between the lasers on the modulation response of solitary two-element laser arrays. In particular, we consider four different waveguide structures that have been introduced in our prior work [43] and modulate the phased array in phase or out of phase by following the modulation schemes proposed in Ref. [27]. We identify interesting differences in the modulation response under in-phase and out-of-phase modulation in the four cases of waveguide structures considered, and the important role played by the laser separation and frequency offset. We also compare these modulation schemes to the case of modulating only one element of the phased array. Second, we follow the approach widely employed to enhance the modulation bandwidth of single emitters [14,15] by examining the effect of introducing optical injection locking. Specifically, we consider both in-phase and out-of-phase modulation as well as master amplitude modulation of optically injected two-element phased arrays. Previous work [25] considered the case of strongly optically coupled VCSELs in an array in which they are modulated as monolithic mutual injection-locked lasers; modeling of this was based on well-established injection-locking laser rate equations. In contrast we deal with a phased array operating in a weak coupling regime, and we model this using coupled mode rate equations, thereby accounting for evanescent coupling between electric fields, in conjunction with complex coupling coefficients. We also note previous work reported in Ref. [27] and our work differs from this in four important aspects: (i) the inclusion of the frequency offset between the two lasers that inevitably occurs in practice; (ii) the calculation of real and imaginary parts of the complex coupling coefficient from the specific gain and index differences in the four waveguide structures considered; (iii) the simulation using the full rate equations that allows us to extract stability diagrams before modulation is applied to the phased array; and (iv) the inclusion of additional schemes for further improving the modulation bandwidth. By taking this approach we provide a more comprehensive study on the modulation properties of phased-array semiconductor lasers utilizing coupled mode rate equations.

The contents of this paper are organized as follows. In Section 2 we introduce the model including the equations for the solitary and optically injected two-element semiconductor laser phased array, the waveguide structures, and device parameters considered in the current study. Section 3 is devoted to the results for the modulation response of the phased array operating in the cases with and without optical injection. Finally, our basic conclusions are given in Section 4.

2. THEORETICAL MODEL

We focus on the simplest case of the two-element phased laser array operating in a weak coupling regime, whose schematic is shown in Fig. 1. Following our prior work [43], we restrict our attention to a semiconductor laser array, which consists of two identical laser waveguides, A and B; individually each is of width $2a$ and symmetric about their centers. A and B are separated edge-to-edge by distance $2d$ and mutually coupled through the evanescent tails of their fields. The dynamics of such a configuration can be modeled based on rate equations using coupled mode theory [31–33]. Because of its simplicity and the physical insight that it offers, we will use this coupled mode model to study the modulation properties of a two-element phased array in some detail. Additionally, we shall investigate the effect of simultaneous optical injection on the modulation response of such a phased-array system, where both lasers within the array are subject to identical external injection.

The rate equations of a phased array under external injection are of the following form [49]:

$$\frac{d\tilde{E}_A}{d\tilde{t}} = \Gamma\frac{c}{2n_g}a_{\text{diff}}(\tilde{N}_A - \tilde{N}_{A\text{th}})(1 - i\alpha_H)\tilde{E}_A + i(\omega - \tilde{\Omega}_A)\tilde{E}_A + i\eta\tilde{E}_B + k_{\text{inj}}\tilde{E}_{\text{inj}}e^{-i(\omega_{\text{inj}}-\omega)t}, \quad (1)$$

$$\frac{d\tilde{E}_B}{d\tilde{t}} = \Gamma\frac{c}{2n_g}a_{\text{diff}}(\tilde{N}_B - \tilde{N}_{B\text{th}})(1 - i\alpha_H)\tilde{E}_B + i(\omega - \tilde{\Omega}_B)\tilde{E}_B + i\eta\tilde{E}_A + k_{\text{inj}}\tilde{E}_{\text{inj}}e^{-i(\omega_{\text{inj}}-\omega)t}, \quad (2)$$

$$\frac{d\tilde{N}_{A,B}}{d\tilde{t}} = P_{A,B} - \tilde{N}_{A,B}\gamma_N - \frac{c}{n}[g_{\text{th}} + a_{\text{diff}}(\tilde{N}_{A,B} - \tilde{N}_{A,B\text{th}})]|\tilde{E}_{A,B}|^2. \quad (3)$$

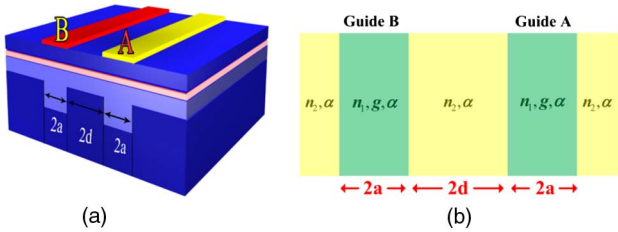

Fig. 1. (a) Schematic of a phased array consisting of two laser waveguides, A and B, with each of width $2a$ and an edge-to-edge separation of $2d$. (b) More details about the distribution of refractive indices $n_{1,2}$, where g represents gain per unit length and α the background attenuation coefficient per unit length due to effects such as scattering and intervalence band absorption [43].

This model can be seen as an extension of the coupled laser model used in our prior work [43], where the subscript A/B stands for laser A/B, $\tilde{E}_{A,B}$ are the electric fields, and $\tilde{N}_{A,B}$ are the carrier concentrations (with the subscript 'th' indicating the threshold values). The third terms on the right side of the first two equations stand for the lateral-coupling effect between the two identical lasers of the phased array, with η the complex coupling rate. This rate is expressed in terms of amplitude and phase parameters C_η, C_θ (found from numerical integration)

$$|\eta| = C_\eta \exp\left(-2W_r\frac{d}{a}\right), \qquad \arg(\eta) = C_\theta - 2W_i\frac{d}{a}, \tag{4}$$

where W_r, W_i are the real and imaginary parts of the transverse propagation constant in the regions outside the cores of waveguides A and B. The last terms in Eqs. (1) and (2) represent the external injection from a master laser, where ω_{inj} is the injected angular frequency and ω the free-running angular frequency of the total electric field of the phased array in the absence of injection, $\tilde{E}_{\text{inj}}$ the injected field, and k_{inj} a coupling rate for the injected signal. On the contrary, for a solitary phased array, the last terms in Eqs. (1) and (2) should not be taken into account. Other parameters are the optical confinement factor Γ, the speed of light c, the group index n_g, the differential gain a_{diff}, the linewidth enhancement factor α_H, the cavity resonance frequencies $\tilde{\Omega}_{A,B}$, the pump rate $P_{A,B}$, the carrier decay rate γ_N, the refractive index n, and the threshold gains g_{th}, which are assumed equal and given by the relation $\Gamma g_{\text{th}} = n_g/(c\tau_p)$, where τ_p is the photon lifetime. It follows from this that $\tilde{N}_{A\text{th}} = \tilde{N}_{B\text{th}} \equiv \tilde{N}_{\text{th}}$.

For convenience, we carried out a normalization process that adopts the normalizations and definitions of variables

$$E_{A,B} = \frac{\tilde{E}_{A,B}}{|\tilde{E}_o|}; \quad N_{A,B} = \frac{\tilde{N}_{A,B}}{\tilde{N}_{\text{th}}} - 1; \quad t = \gamma_N \tilde{t};$$
$$\beta = \frac{c}{2n_g\gamma_N}\Gamma a_{\text{diff}}\tilde{N}_{\text{th}}; \quad V = \frac{\omega}{\gamma_N}; \quad \Omega_{A,B} = \frac{\tilde{\Omega}_{A,B}}{\gamma_N};$$
$$\kappa = \frac{\eta}{\gamma_N}; \quad K = \frac{k_{\text{inj}}\tilde{E}_{\text{inj}}}{|\tilde{E}_0|\gamma_N}; \quad \Delta = \frac{\omega_{\text{inj}} - \omega}{\gamma_N};$$
$$G_{\text{th}} = \frac{|\tilde{E}_o|^2 c}{n\tilde{N}_{\text{th}}\gamma_N}g_{\text{th}}; \quad \zeta = \frac{|\tilde{E}_o|^2 c}{n\gamma_N}a_{\text{diff}}; \quad \mu_{A,B} = \frac{P_{A,B}}{\gamma_N\tilde{N}_{\text{th}}} - 1, \tag{5}$$

where $|\tilde{E}_0|$ is the amplitude of the electric field for a free-running laser.

Substituting Eq. (5) into Eqs. (1)–(3), we obtain the following set of normalized equations to describe the dynamics and modulation properties of solitary and optically injected phased-array semiconductor lasers:

$$\frac{dE_A}{dt} = \beta N_A(1 - i\alpha_H)E_A + i(V - \Omega_A)E_A + i\kappa E_B + Ke^{-i\Delta t}, \tag{6}$$

$$\frac{dE_B}{dt} = \beta N_B(1 - i\alpha_H)E_B + i(V - \Omega_B)E_B + i\kappa E_A + Ke^{-i\Delta t}, \tag{7}$$

$$\frac{dN_{A,B}}{dt} = \mu_{A,B} - N_{A,B} - (G_{\text{th}} + \zeta N_{A,B})|E_{A,B}|^2. \tag{8}$$

Equations (6) and (7) contain explicit time dependence (nonautonomous). To get rid of it, we introduce new variables $E_I = E_A e^{i\Delta t}$ and $E_{II} = E_B e^{i\Delta t}$. Further, we rewrite these equations in terms of the real and imaginary parts of the complex electric fields, i.e., $E_I = E_x + iE_y$ and $E_{II} = E_m + iE_n$. The resulting rate equations are written as

$$\frac{dE_x}{dt} = \beta N_A(E_x + \alpha_H E_y) - (V - \Omega_A)E_y - (E_n\kappa_R + E_m\kappa_I) + K - \Delta E_y, \tag{9}$$

$$\frac{dE_y}{dt} = \beta N_A(E_y - \alpha_H E_x) + (V - \Omega_A)E_x + (E_m\kappa_R - E_n\kappa_I) + \Delta E_x, \tag{10}$$

$$\frac{dE_m}{dt} = \beta N_B(E_m + \alpha_H E_n) - (V - \Omega_B)E_n - (E_y\kappa_R + E_x\kappa_I) + K - \Delta E_n, \tag{11}$$

$$\frac{dE_n}{dt} = \beta N_B(E_n - \alpha_H E_m) + (V - \Omega_B)E_m + (E_x\kappa_R - E_y\kappa_I) + \Delta E_m, \tag{12}$$

$$\frac{dN_A}{dt} = \mu_A - N_A - (G_{\text{th}} + \zeta N_A)(E_x^2 + E_y^2), \tag{13}$$

$$\frac{dN_B}{dt} = \mu_B - N_B - (G_{\text{th}} + \zeta N_B)(E_m^2 + E_n^2), \tag{14}$$

where the normalized complex coupling coefficient is written in terms of its real and imaginary parts $\kappa = \kappa_R + \kappa_I$.

In our numerical simulations, a fourth-order Runge–Kutta algorithm has been used to solve Eqs. (9)–(14). The following set of parameter values is considered: $\alpha_H = 2$, $a = 4$ μm, $a_{\text{diff}} = 2.5 \times 10^{-16}$ cm^2, $N_o = 1 \times 10^{18}$ cm^{-3}, $\gamma_N = 1.0$ ns^{-1}, $\tau_p = 1.53$ ps, and $n = 3.4$. These values are fixed throughout the current study as they are assumed to be representative of those for two-element mutually coupled phased-laser arrays. All these parameter values are the same as those given in Refs. [42,43,48,49], except for the differential gain a_{diff}. Here a smaller differential gain is chosen such that a smaller value of the relaxation oscillation frequency is obtained; this will be used to compare with the resonance frequency in the case of out-of-phase modulation. We restrict attention to the case of homogeneous pumping in each laser, so that $\mu \equiv \mu_A = \mu_B$. For consistency we study the influence of waveguiding structures based on the cases analyzed in Ref. [43], summarized below in Table 1, where Δn_r and Δn_i are the real and imaginary parts of the index difference between the core and cladding regions of the waveguides. The first is purely real index guiding, the second positive index guiding with gain-guiding, the third pure gain-guiding (no built-in index guiding), and the last index antiguiding with gain-guiding. In all these cases the analysis

Table 1. Values of Key Parameters for Modeling, Using Material Parameter Values Given in Refs. [43,48]

Δn_r	g_{th} (cm^{-1})	Δn_i	W_r	W_i	Γ	C_η (ns^{-1})	C_θ (rad)
0.00097	87.7	0	1.26	0	0.844	83.6	0
0.0005	90.6	0.000937	1.09	0.896	0.817	90.2	0.233
0	99.3	0.00103	0.795	1.22	0.745	91.9	0.294
−0.0005	108	0.00112	0.604	1.61	0.685	96.3	0.183

of the wave guiding properties assumes that both the individual guides and overall array are symmetric and hence that the two lasers are nominally identical. Nevertheless, we do allow for a static difference in lasing frequency [$\Delta\Omega/2\pi = (\Omega_B - \Omega_A)/2\pi$] between them that might occur in practice either unintentionally as a result of small fabrication variations or by design. We refer to this as the "offset frequency", or simply as the "offset" [42].

3. NUMERICAL RESULTS AND DISCUSSION

In this section we will focus on the presentation of numerical results and discussion based on the model in Section 2. To perform a small signal modulation, we have to obtain the location of the continuous wave states (stationary operation regimes) in the parameter space. In the case of the solitary phased array, the parameter space is composed of the laser separation ratio d/a, which controls the coupling strength, and the frequency offset $\gamma_N\Delta\Omega/2\pi$. In the optical injection case, we present their location in terms of the injection ratio K against the frequency detuning $\Delta f = \gamma_N\Delta/2\pi$. To this end, one could carry out a detailed bifurcation analysis to obtain high-resolution bifurcation diagrams accounting for all the dynamical regimes, such as stationary, period one, period two, higher periodic, quasiperiodic, and even chaotic states, as we did in our previous publications [42,50]. However, here we are interested to know only the location of the stationary operational regimes (regardless of in-phase or out-of-phase equilibrium points that have been clarified in Ref. [43]), and hence we turn to the simple stability diagram distinguishing only stability and instability.

A. Modulation Properties of a Solitary Two-Element Phased Array

Figure 2 presents the stability maps in the (d/a, $\gamma_N\Delta\Omega/2\pi$) plane for two different but fixed pump rates, i.e., $P = 1.1P_{th}$ and $P = 2P_{th}$, in the four waveguide structures outlined in the preceding section. For illustrative purposes, the steady-state regions are shown in blue, while the unstable regions are represented in yellow. Note that in-phase and out-of-phase solutions are not distinguished here since this is not important for the current study. At first, let us consider $P = 1.1P_{th}$. For the purely real index guide, Fig. 2(a) shows that the phased array is unstable over an extremely large portion of the parameter space and the limited stable region is not useful for bandwidth enhancement, as will be shown below. This is consistent with the claim for $\kappa_I = 0$ in Ref. [27]. The stability map for the positive index guiding with gain-guiding is shown in Fig. 2(b), which clearly indicates the appearance of a second stable island of interest for smaller values of d/a. In the cases of pure gain-guiding and index antiguiding with gain-guiding, the stable regions greatly expand (a wider range on the vertical axis is used) and more separate islands corresponding to stability appear, as shown in Figs. 2(c) and 2(d). This is in good agreement with the periodicity behavior with laser separation revealed by using linear stability analysis and a continuation technique. The results for $P = 2P_{th}$ are shown in Figs. 2(e)–2(h). It can be clearly seen that the pump has no significant influence on the stability regions in terms of their size, location, or number.

In the following we numerically investigate modulation response of the solitary two-element phased array by sinusoidally modulating the pump current in Eqs. (13) and (14) as

$$\mu(t) = \mu_{A,B}\left[1 + mL_{A,B}\sin\left(2\pi f_m \frac{t}{\gamma_N}\right)\right], \tag{15}$$

where $\mu_{A,B}$ is the bias current without modulation, m is the modulation index, f_m is the modulation frequency, and $L_{A,B} = \pm 1$ allows the array elements to be modulated in phase or out of phase with respect to each other. In a stable region as indicated in Fig. 2, periodic modulation of the pump current of the array (the input signal) can entrain a limit cycle in the output signal at the same frequency, but the amplitude is frequency dependent. In this way, we can define the modulation response as $M = (S_{max} - S_{min})/m\mu_{A,B}$, where S_{max} and S_{min} stand for

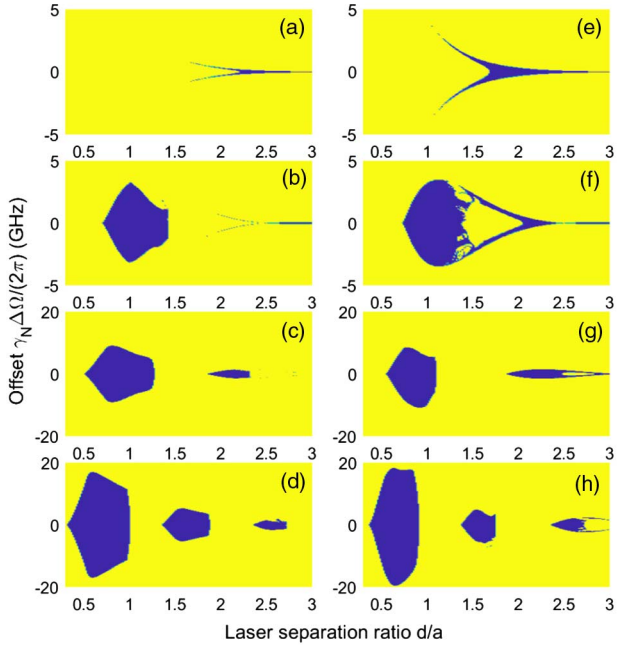

Fig. 2. Stability diagrams of the solitary phased array in the (d/a, $\gamma_N\Delta\Omega/2\pi$) plane for (a)–(d) $P = 1.1P_{th}$ and (e)–(h) $P = 2P_{th}$. (a), (e) Purely real index, (b), (f) positive index guiding with gain-guiding, (c), (g) pure gain-guiding, and (d), (h) index antiguiding with gain-guiding. Blue (yellow) stands for stability (instability).

the maximum and minimum of the intensity of the laser output, respectively. In all the numerical simulations, the modulation index is set to be $m = 0.02$ in accordance with small signal modulation; the modulation response is normalized by the value at the lowest modulation frequency (0.1 GHz). It should be noted that for simultaneous modulation $|L_{A,B}| = 1$, the calculated modulation responses for lasers A and B are nearly identical, and so only the results for laser A are shown; no frequency offset is included, unless otherwise noted.

Let us first consider the modulation response for $P = 1.1P_{\text{th}}$; the corresponding results are shown in Fig. 3. The relaxation oscillation frequency f_R is given by [43]

$$(2\pi f_R)^2 = \mu\frac{\gamma_N}{\tau_p}(C_Q + 1) - \gamma_D^2, \tag{16}$$

where γ_D is the damping rate given by

$$\gamma_D = -\frac{\gamma_N}{2}[1 + \mu(C_Q + 1)], \tag{17}$$

and C_Q is defined as

$$C_Q = N_o\frac{a_{\text{diff}}}{g_{\text{th}}}. \tag{18}$$

At the pump rate of $P = 1.1P_{\text{th}}$ ($\mu = 0.1$), the relaxation oscillation frequency f_R is ~2.3 GHz. For free-running operation of the laser, the strongest modulation response should be located at this carrier–photon resonance frequency, which is also the case for our solitary phased array under in-phase modulation. As can be seen from Fig. 3, the response to in-phase modulation is identical to that of a single solitary laser (not shown), regardless of the waveguide structure. This is expected since the analytical approximation of in-phase modulation response given in Ref. [27] does not include any dependence on κ_R, which is proportional to the rate of exchange of photons (beating) between the lasers and thus is expected to give a high-frequency response. On the contrary, the response to out-of-phase modulation is very dependent on the waveguide parameters. Using the information on the stability properties shown in Fig. 2, we have conducted extensive simulations and Fig. 3 presents the most promising response to out-of-phase modulation where a higher resonance frequency can be seen for each structure. It is clear that the purely real index guide [Fig. 3(a)] and the positive index guiding with gain-guiding [Fig. 3(b)] cannot offer bandwidth enhancement through out-of-phase modulation. The reason is that in the stable regions the resulting resonance frequency (due to photon–photon resonance effect) is much less than f_R for these two waveguide structures. In contrast, for the other two cases as shown in Figs. 3(c) and 3(d), a much higher resonance frequency is obtained for the out-of-phase modulation, especially for index antiguiding with gain-guiding [see Fig. 3(d)], where we obtain $f_{\text{PP}} = \gamma_N|\kappa_R|/\pi = 9.03$ GHz. This is considerably greater than f_R, and thus a strong response to out-of-phase modulation close to f_{PP} is expected. In Ref. [27], first-order corrections to the expression $f_{\text{PP}} = \gamma_N|\kappa_R|/\pi$ are derived, and these can account for the fact that the peak of the strong high-frequency response is not located exactly at f_{PP} in Fig. 3.

To confirm our results shown in Fig. 3, Fig. 4 depicts the calculated modulation response for the four waveguide structures in the case of $P = 2P_{\text{th}}$ ($\mu = 1$). Again, by selecting the laser separation ratio d/a, the best performance for each structure at this pump rate is shown. According to the equation above, the relaxation oscillation frequency is estimated to be $f_R \approx 7.4$ GHz. As can be seen from Figs. 4(a) and 4(b), in-phase and out-of-phase modulations lead to almost identical response with a resonance peak at f_R, meaning no improvement either in the resonance frequency or in the modulation bandwidth can be obtained when using these design parameters. However, as shown in Figs. 4(c) and 4(d), the results for the other two waveguide structures clearly show that the resonance peak for out-of-phase modulation is shifted to a higher frequency close to $f_{\text{PP}} = \gamma_N|\kappa_R|/\pi$ for the same reason given above, when compared to the case of in-phase modulation.

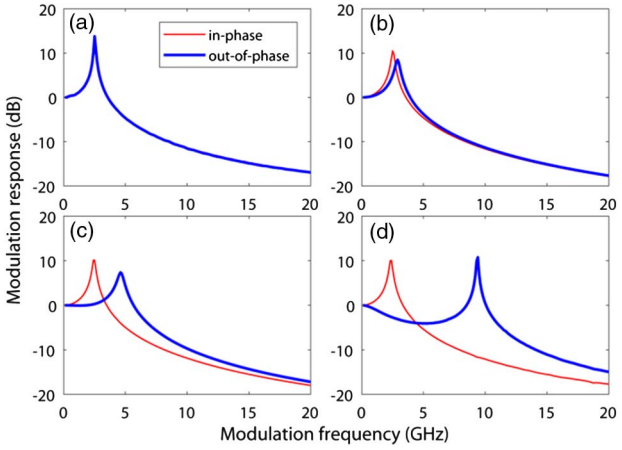

Fig. 3. Modulation frequency response of the solitary phased array at $P = 1.1P_{\text{th}}$. (a) Purely real index with $d/a = 2.4$, (b) positive index guiding with gain-guiding with $d/a = 1.35$, (c) pure gain-guiding with $d/a = 1.25$, and (d) index antiguiding with gain-guiding with $d/a = 1.01$. Red (blue) represents in-phase (out-of-phase) modulation.

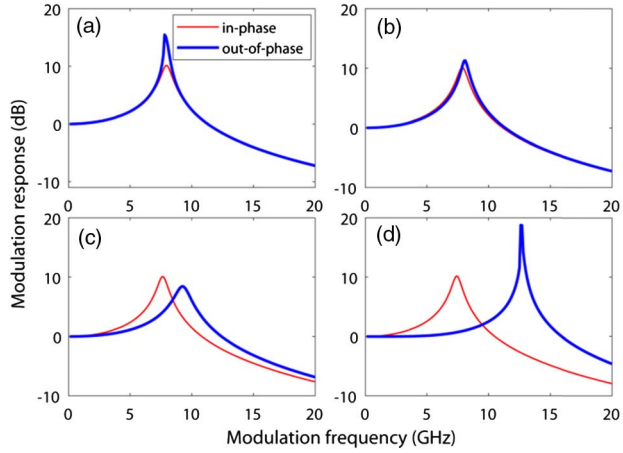

Fig. 4. Modulation frequency response of the solitary phased array at $P = 2P_{\text{th}}$. (a) Purely real index with $d/a = 1.75$, (b) positive index guiding with gain-guiding with $d/a = 1.3$, (c) pure gain-guiding with $d/a = 1.05$, and (d) index antiguiding with gain-guiding with $d/a = 0.91$. Red (blue) represents in-phase (out-of-phase) modulation.

These observations agree well with those in Fig. 3. It is worth noting that a combination of index antiguiding and gain-guiding offers higher resonance frequencies in the case of out-of-phase modulation, but a frequency dip between dc and resonance might occur for lower pump rates. For instance, as can be seen from Fig. 3(d), the dc-to-resonance dip in the case of out-of-phase modulation extends to below the –3 dB line and thus results in poor 3 dB bandwidth, even though the photon–photon resonant effect pushes the resonance frequency to a higher value compared to the in-phase modulation. The occurrence of a preresonance frequency dip limiting the 3 dB bandwidth has also been reported in optical injection systems, where the cause has been elucidated [14]. The suggested ways to mitigate this dip include increasing the photon density of the cavity by increased pump current [14,15] as well as taking into account the combination effects of optical injection and gain lever [16,17]. Indeed, as shown in Fig. 4(d) for a higher pump level, the absence of the dc-to-resonance dip confirms that increasing pump rate is an effective way to suppress the low-frequency drop-off and improve the 3 dB bandwidth in the phased array.

As discussed in Ref. [27], the real part κ_R of the complex coupling coefficient determines the frequency of peak response to out-of-phase modulation, while the imaginary part κ_I has a strong influence on the modulation efficiency (higher resonance peak). Thus, it would be of interest to know the impact of the complex coupling coefficient in terms of the variation of the laser separation ratio d/a for specific structures. From the results presented above, it can be anticipated that the structure combining the index antiguiding with gain-guiding offers better performance for maximizing resonance frequency and enhancing modulation bandwidth. Hence, we will focus on this structure, unless otherwise specified. As an example, Fig. 5 illustrates the impact of the laser separation on modulation response of the phased array for $P = 1.1P_{\text{th}}$ and $P = 2P_{\text{th}}$. In the case of in-phase modulation, the response is robust to the variation of d/a, as can be expected from the results in Figs. 3 and 4. In contrast to in-phase modulation, simulations point out that the response to out-of-phase modulation is extremely sensitive to d/a. The results imply that a reasonable value of d/a should be chosen to balance the resonance frequency and the modulation efficiency (responsivity) and to achieve desired modulation properties. When optimized, a resonance peak with enhanced amplitude at a high frequency can be obtained in the modulation response curves, as shown in Figs. 5(b) and 5(d). Again, the frequency dip is present for $P = 1.1P_{\text{th}}$ [see Fig. 5(b)] but disappears for $P = 2P_{\text{th}}$ [see Fig. 5(d)], confirming our previous assessment.

The analysis presented so far has assumed an ideal phased array with no frequency offset between the two elements. However, in practical applications fabrication imperfections may lead to spectral offset among the array elements, which can degrade the array coherence. Thus, it is of importance to investigate the impact of the frequency offset on the modulation properties of the phase array. As an example, Figs. 6(a) and 6(b) display the modulation response to in-phase and out-of-phase modulation, respectively, for a range of offset frequencies when $P = 1.1P_{\text{th}}$ and $d/a = 0.97$. For comparison, the results for zero offset are also depicted. In the case of in-phase modulation, the position of the resonance peak and the peak amplitude remain unchanged by varying the offset [Fig. 6(a)]. In comparison, the offset has a significant impact on the modulation properties of the phased array when the two elements are modulated out of phase relative to each other, as shown in Fig. 6(b). It can be seen that another resonance peak arises due to the presence of the offset, leading to double peak response curves. As the offset becomes greater, the amplitude of both resonance peaks is enhanced gradually. However, the position of the lower resonance peak is not sensitive to the offset while that of the second is only very weakly so. This can be attributed to the fact that the first resonance peak arises from the carrier–photon interaction, and the second one stems from the photon–photon resonant effect; thus, the finite offset considered here has little or no effect on either of them. Additionally, the frequency dip between the two resonant peaks

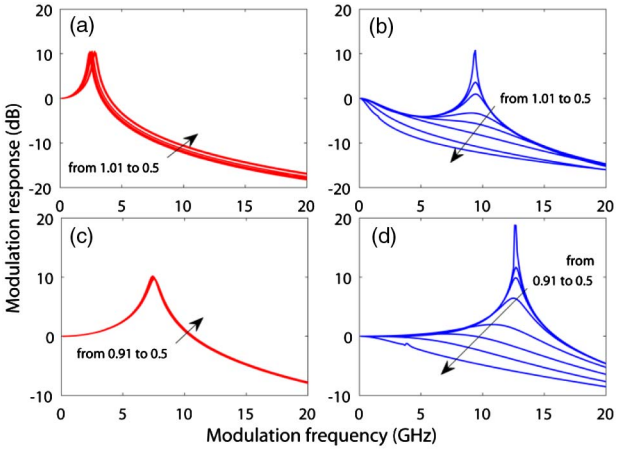

Fig. 5. Modulation frequency response of the solitary phased array at (a), (b) $P = 1.1P_{\text{th}}$ and (c), (d) $P = 2P_{\text{th}}$ for index antiguiding with gain-guiding. (a), (b) d/a, 0.5–1.01 and (c), (d) d/a, 0.5–0.91. (a), (c) In-phase modulation and (b), (d) out-of-phase modulation.

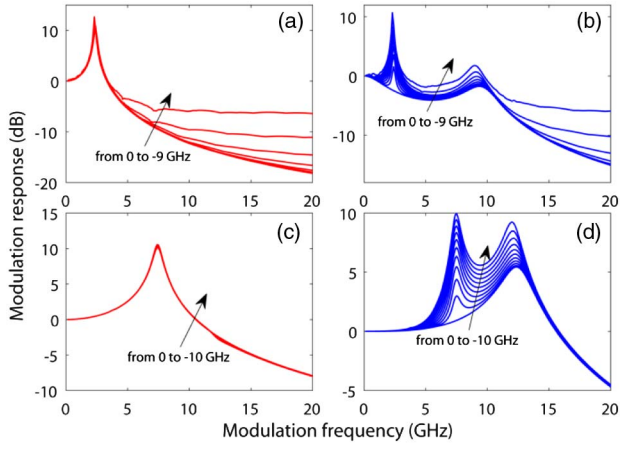

Fig. 6. Modulation frequency response of the solitary phased array for (a), (b)$P = 1.1P_{\text{th}}$ and $d/a = 0.97$, as well as (c), (d) $P = 2P_{\text{th}}$ and $d/a = 0.87$ in the case of index antiguiding with gain-guiding. (a), (b) $\gamma_N \Delta\Omega/2\pi$, 0 to –9 GHz and (c), (d) $\gamma_N \Delta\Omega/2\pi$, 0 to –10 GHz. (a), (c) In-phase modulation and (b), (d) out-of-phase modulation.

will be reduced with increasing offset, which is beneficial to the modulation bandwidth enhancement. Similar trends can be seen for both modulation schemes at higher pump rates. A typical example is shown in Figs. 6(c) and 6(d), where $P = 2P_{th}$ and $d/a = 0.87$. However, at a higher pump rate only a small increase in bandwidth is seen with reference to the −3 dB line, which arises from the interaction of the responses due to two characteristic frequencies. Further, we must emphasize that in the case of phased arrays, the offset should be limited to a small range guided by a consideration of the stability properties as indicated in Fig. 2. This is distinct from the case of optical injection systems [11–22], where a very large detuning frequency is allowed and the resonance frequency is roughly proportional to the detuning.

Thus far, we considered the case of simultaneous current modulation $|L_{A,B}| = 1$, either in phase or out of phase. We now consider the situation where only one element of the phased array is sinusoidally modulated [23]. We assume that the current of laser A is modulated, while laser B is pumped only by a CW current, that is, $L_A = 1$ and $L_B = 0$. For both lasers, the modulation response is normalized by the value at the lowest modulation frequency (0.1 GHz) of laser A. Figure 7 presents typical examples for single current modulation at two pump rates, i.e., $P = 1.1P_{th}$ and $P = 2P_{th}$. Double peak response curves are seen in the response of both lasers of the phased array. Moreover, it should be noted that at the two resonant frequencies, the resonance amplitudes of lasers A and B are almost the same, despite that only the current of laser A is sinusoidally modulated. The appearance of two resonant peaks in the modulation response curve is in good agreement with the modulation properties observed in mutually coupled integrated distributed feedback lasers [23] and twin-square microcavity lasers [26] as well as coherently coupled phased photonic crystal VCSEL arrays [25], where small-signal modulation is applied to only one element of the array.

In terms of a broadband source, it should be noted that achievable modulation bandwidth for these waveguide parameters is not high because these structures are not optimized and the resulting resonance frequency $f_{PP} = \gamma_N|\kappa_R|/\pi$ is far below 20 GHz. A straightforward approach to enhancing this is to further optimize the device by carefully considering index guiding, gain-guiding, and their combination, an aim for future work. However, we next consider a different approach by introducing external injection into the phased array to enhance the modulation properties. The aim here is to significantly increase the resonance frequency and hence the corresponding modulation bandwidth [14,15] via external optical injection.

B. Modulation Properties of an Optically Injected Two-Element Phased Array

We now concentrate on the case of the two elements of the phased array under simultaneous external injection [49]. Without loss of generality, we consider index antiguiding with gain-guiding for zero offset, i.e., both lasers in the array are identical. In fact, the findings in this subsection also hold for other structures and nonzero offset. Again, before modulating, stability diagrams are used to distinguish the locked (blue) and unstable (yellow) regions.

In Figs. 8(a) and 8(b), we show the stability maps for $P = 1.1P_{th}$ and $d/a = 1.01$, as well as for $P = 2P_{th}$ and $d/a = 0.91$, respectively. In both cases considered here, the two lasers of the array can be simultaneously locked in the same region indicated in blue, and thus only the response for laser A is shown. In our previous work, we have carried out a comprehensive study on the locking conditions and gained a better understanding of the mechanisms, the injection-locking characteristics, and the effects of some key parameters on the locking region for the case of simultaneous or single external injection [48,49]. The results suggested the locking behavior in each injection scheme is not restricted by waveguiding structure but revealed a generic locking behavior. Here we emphasize that only the shape of the locking region is wide and resembles that of a single laser subject to external injection. Hence, we expect that the phased array under simultaneous injection should share some other features with an optically injected laser, for example, the modulation properties that will be studied here in some detail.

We consider the in-phase and out-of-phase current modulation of the phased array under external injection. It has been demonstrated that increasing the frequency detuning and/or the injection ratio will lead to the enhancement of the resonance frequency in a single laser subject to external injection [14,15]. Thus, here we investigate if this holds true for the array. Figure 9 shows the effect of the frequency detuning on the modulation response. In particular, Figs. 9(a) and 9(b), respectively, illustrate the response to in-phase and out-of-phase modulation for a range of detuning frequencies at a fixed injection ratio $K = 200$ and pump level $P = 1.1P_{th}$.

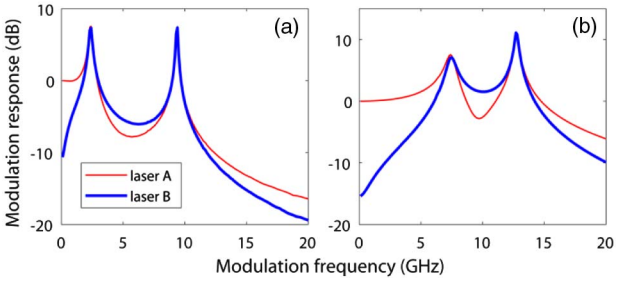

Fig. 7. Modulation frequency response of the solitary phased array for (a) $P = 1.1P_{th}$ and $d/a = 1.01$, as well as (b) $P = 2P_{th}$ and $d/a = 0.91$ in the case of index antiguiding with gain-guiding. Red (blue) represents laser A (B). Here only laser A is modulated.

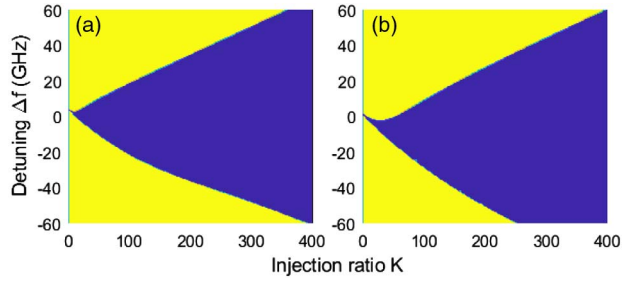

Fig. 8. Stability diagrams of the optically injected phased array in the $(K, \Delta f)$ plane for (a) $P = 1.1P_{th}$ and $d/a = 1.01$, as well as for (b) $P = 2P_{th}$ and $d/a = 0.91$ in the case of index antiguiding with gain-guiding. Blue (yellow) stands for stability (instability).

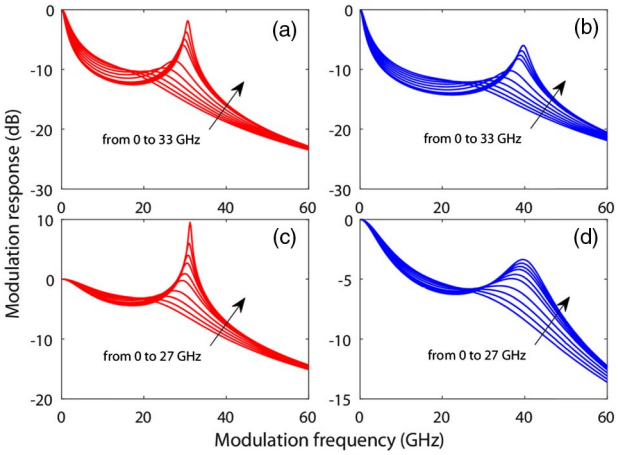

Fig. 9. Modulation frequency response of the optically injected phased array for different detuning frequencies Δf and a fixed injection ratio $K = 200$ in the case of index antiguiding with gain-guiding, where (a), (b) $P = 1.1P_{\text{th}}$ and $d/a = 1.01$, as well as (c), (d) $P = 2P_{\text{th}}$ and $d/a = 0.91$. (a), (c) In-phase modulation and (b), (d) out-of-phase modulation.

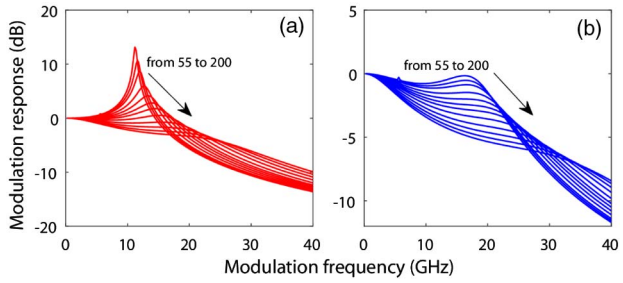

Fig. 10. Modulation frequency response of the optically injected phased array for different injection ratios K and a fixed detuning frequency $\Delta f = 0$ GHz in the case of index antiguiding with gain-guiding, where $P = 2P_{\text{th}}$ and $d/a = 0.91$. (a) In-phase modulation and (b) out-of-phase modulation.

Several features can be summarized as follows. First, the general trends are similar for in-phase and out-of-phase modulation. In other words, as the detuning increases, both the resonant frequency and the peak amplitude are enhanced, while a larger dc-to-resonance dip can be observed, limiting the 3 dB bandwidth. Second, the results show that the position of the resonance frequency is always at a higher frequency when applying out-of-phase modulation. This can be attributed to the shift originating from the photon–photon resonant effect when the phased array is modulated out of phase as was discussed in the solitary case. Third, these observations agree well with those in an optically injected laser [11–22]. Therefore, the modulation properties of the optically injected phased array can be easily understood. Figures 9(c) and 9(d) show a similar response for a range of detuning frequencies but at a pump level $P = 2P_{\text{th}}$. When a higher pump rate is considered, simulations show that the undesirable dc-to-resonance dip is reduced, thus allowing a larger 3 dB bandwidth. The reason for this enhancement mentioned in the preceding section has been extensively discussed in other optical injection systems [14,15].

We next study the influence of the injection ratio K on the modulation properties. As an example, Fig. 10 shows the results for $P = 2P_{\text{th}}$ and zero detuning: in-phase and out-of-phase modulation. In both modulation schemes, as the injection ratio is increased, the position of the resonance frequency is shifted to a higher frequency range, but the response becomes more damped. This also coincides with the observations in other optically injected lasers [14,15] and coherently coupled VCSEL arrays [25].

The above discussions indicate that optical injection can indeed enhance the resonance frequency and may result in modulation bandwidth enhancement. To illustrate this point, Fig. 11(a) shows an example for the response curve under appropriate conditions ($P = 2P_{\text{th}}$, $d/a = 0.91$, $\Delta f = 20$ GHz, and $K = 160$). As can be seen from this figure, the 3 dB bandwidth is about 30 GHz for in-phase modulation, more than 4 times the relaxation oscillation frequency of the equivalent free-running laser. However, the bandwidth for out-of-phase modulation is rather low due to the undesirable frequency dip. To improve this, we consider another higher pump rate, $P = 5P_{\text{th}}$, as increasing photon density by higher pump levels has been suggested as an effective way to suppress the dip and increase the bandwidth [14]. To maintain the stability, the injection ratio is increased to $K = 250$, while other parameters are kept constant. The results are shown in Fig. 11(b), where the preresonance dip is lifted above the −3 dB line. Obviously, the resulting bandwidth for in-phase and out-of-phase modulation can be estimated at about 49 GHz and 55 GHz, respectively.

Finally, we also test another approach to improving the resonance frequency and the corresponding bandwidth as previously reported for a single laser subject to external injection. In this method, we modulate the amplitude of the master light before reaching the phased array [15], rather than the laser current modulation used above. A typical example of the modulation response is shown in Fig. 12, where the injection ratio is increased from $K = 160$ to $K = 400$, and other parameters are identical to those in Fig. 11(a). The results reveal that such a master amplitude modulation scheme works effectively in the optically injected phased array and allows a bandwidth above 160 GHz ($K = 400$), more than 5 times that obtained in Fig. 11(a). We would like to point out that these findings

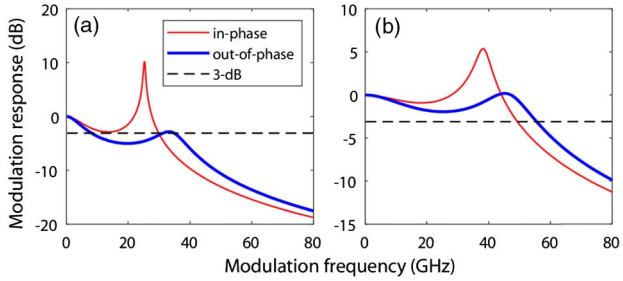

Fig. 11. Modulation frequency response of the optically injected phased array for (a) $P = 2P_{\text{th}}$ and (b) $P = 5P_{\text{th}}$ in the case of index antiguiding with gain-guiding. (a) $K = 160$ and (b) $K = 250$. Other parameters are $d/a = 0.91$ and $\Delta f = 20$ GHz. Red (blue) represents in-phase (out-of-phase) modulation. Horizontal dashed line corresponds to the −3 dB level.

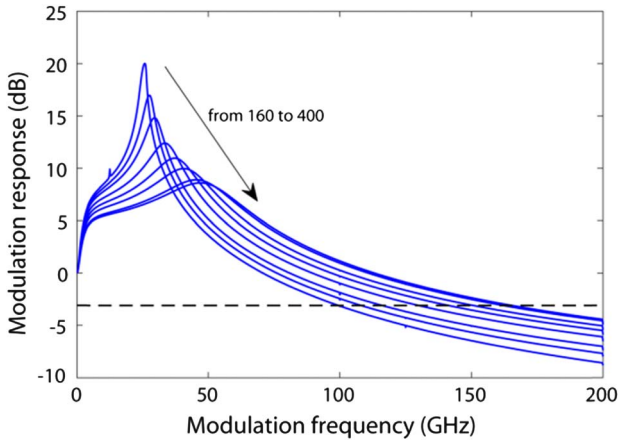

Fig. 12. Modulation frequency response of the master-amplitude-modulated optically injected phased array for different injection ratios K and a fixed detuning frequency $\Delta f = 20$ GHz in the case of index antiguiding with gain-guiding. Other parameters are $P = 2P_{\text{th}}$ and $d/a = 0.91$. Horizontal dashed line corresponds to the –3 dB level.

can directly apply to other waveguide structures and thus are of prime importance for optical communications that require high-speed integrated photonic devices.

4. CONCLUSION

In conclusion, modulation properties of solitary and optically two-element phased-array semiconductor lasers have been numerically studied based on coupled mode rate equations. The stability diagrams distinguishing stable and unstable regions have been calculated and used to guide the small-signal current modulation, which has been carried out within the stationary operation regimes. We have taken into consideration the influence of waveguide structures, the laser separation, and the frequency offset between the two lasers of the array, which was not considered previously. In particular, we have considered four different waveguide structures—purely real index guiding, positive index guiding with gain-guiding, pure gain-guiding and index antiguiding with gain-guiding—and modulated the array either in phase or out of phase within the phase-locked regions. We show the influence of the waveguide structure and, for out-of-phase modulation, how this can be selected for bandwidth enhancement. For example, when the structure is designed as a combination of index antiguiding and gain-guiding, the achievable modulation bandwidth in the case of out-of-phase modulation could be much higher than that when the array elements are modulated in phase. Moreover, we have also analyzed the impact of the laser separation (related to the complex coupling coefficient) and the frequency offset between the lasers of the phased array on the modulation properties. We have presented evidence for the appearance of two resonance peaks, one located at the relaxation oscillation frequency and the other at the position of the photon–photon resonance frequency, due to either the presence of the frequency offset or only modulating one element of the phased array. We have also observed significant improvements in modulation dynamics for the optically injected phased array within the injection locking region, where the 3 dB bandwidth can reach 160 GHz by means of a master amplitude modulation technique under reasonable injection conditions. The current study allows us to gain a better understanding of the modulation properties of the phased array with and without external injection, as well as providing useful guidance in the preliminary design of integrated photonic sources that could be engineered for applications requiring either low bandwidth or high frequency and narrow band.

Funding. Engineering and Physical Sciences Research Council (EPSRC) (EP/M024237/1).

REFERENCES

1. R. S. Tucker, "High-speed modulation of semiconductor lasers," J. Lightwave Technol. **3**, 1180–1192 (1985).
2. X. M. Lv, Y. Z. Huang, L. X. Zou, H. Long, and Y. Du, "Optimization of direct modulation rate for circular microlasers by adjusting mode Q factor," Laser Photon. Rev. **7**, 818–829 (2013).
3. Z. A. Sattar and K. A. Shore, "Analysis of the direct modulation response of nanowire lasers," J. Lightwave Technol. **33**, 3028–3033 (2015).
4. H. Han and K. A. Shore, "Zero crosstalk regime direct modulation of mutually coupled nanolasers," IEEE Photon. J. **9**, 1503412 (2017).
5. K. Ding, J. O. Diaz, D. Bimberg, and C. Z. Ning, "Modulation bandwidth and energy efficiency of metallic cavity semiconductor nanolasers with inclusion of noise effects," Laser Photon. Rev. **9**, 488–497 (2015).
6. H. Dalir and F. Koyama, "29 GHz directly modulated 980 nm vertical-cavity surface emitting lasers with bow-tie shape transverse coupled cavity," Appl. Phys. Lett. **103**, 091109 (2013).
7. L. Fan, G. Q. Xia, X. Tang, T. Deng, J. J. Chen, X. D. Lin, Y. N. Li, and Z. M. Wu, "Tunable ultra-broadband microwave frequency combs generation based on a current modulated semiconductor laser under optical injection," IEEE Access **5**, 17764–17771 (2017).
8. G. Morthier, R. Schatz, and O. Kjebon, "Extended modulation bandwidth of DBR and external cavity lasers by utilizing a cavity resonance for equalization," IEEE J. Quantum Electron. **36**, 1468–1475 (2000).
9. F. L. Wang, X. W. Ma, Y. Z. Huang, Y. D. Yang, J. Y. Han, and J. L. Xiao, "Relative intensity noise in high-speed hybrid square-rectangular lasers," Photon. Res. **6**, 193–197 (2018).
10. M. Radziunas, A. Glitzky, U. Bandelow, M. Wolfrum, U. Troppenz, J. Kreissl, and W. Rehbein, "Improving the modulation bandwidth in semiconductor lasers by passive feedback," IEEE J. Sel. Top. Quantum Electron. **13**, 136–142 (2007).
11. T. B. Simpson and J. M. Liu, "Small-signal analysis of modulation characteristics in a semiconductor laser subject to strong optical injection," IEEE J. Quantum Electron. **32**, 1456–1468 (1996).
12. A. Murakami, K. Kawashima, and K. Atsuki, "Cavity resonance shift and bandwidth enhancement in semiconductor lasers with strong light injection," IEEE J. Quantum Electron. **39**, 1196–1204 (2003).
13. N. H. Zhu, W. Li, J. M. Wen, W. Han, W. Chen, and L. Xie, "Enhanced modulation bandwidth of a Fabry–Perot semiconductor laser subject to light injection from another Fabry–Perot laser," IEEE J. Quantum Electron. **44**, 528–535 (2008).
14. E. K. Lau, H. K. Sung, and M. C. Wu, "Frequency response enhancement of optical injection-locked lasers," IEEE J. Quantum Electron. **44**, 90–99 (2008).
15. E. K. Lau, L. J. Wong, X. X. Zhao, Y. K. Chen, C. J. Chang-Hasnain, and M. C. Wu, "Bandwidth enhancement by master modulation of optical injection-locked lasers," J. Lightwave Technol. **26**, 2584–2593 (2008).
16. J. M. Sarraute, K. Schires, S. LaRochelle, and F. Grillot, "Enhancement of the modulation dynamics of an optically injection-locked semiconductor laser using gain lever," IEEE J. Sel. Top. Quantum Electron. **21**, 1801408 (2015).

17. J. M. Sarraute, K. Schires, S. LaRochelle, and F. Grillot, "Effects of gain nonlinearities in an optically injected gain lever semiconductor laser," Photon. Res. **5**, 315–319 (2017).
18. L. Chrostowski and W. Shi, "Monolithic injection-locked high-speed semiconductor ring lasers," J. Lightwave Technol. **26**, 3355–3362 (2008).
19. L. Chrostowski, B. Faraji, W. Hofmann, M. C. Amann, S. Wieczorek, and W. W. Chow, "40 GHz bandwidth and 64 GHz resonance frequency in injection-locked 1.55 μm VCSELs," IEEE J. Sel. Top. Quantum Electron. **13**, 1200–1208 (2007).
20. D. Parekh, X. X. Zhao, W. Hofmann, M. C. Amann, L. A. Zenteno, and C. J. Chang-Hasnain, "Greatly enhanced modulation response of injection-locked multimode VCSELs," Opt. Express **16**, 21582–21586 (2008).
21. C. Wang, M. E. Chaibi, H. M. Huang, D. Erasme, P. Poole, J. Even, and F. Grillot, "Frequency-dependent linewidth enhancement factor of optical injection-locked quantum dot/dash lasers," Opt. Express **23**, 21761–21770 (2015).
22. C. Wang, F. Grillot, V. I. Kovanis, J. D. Bodyfelt, and J. Even, "Modulation properties of optically injection-locked quantum cascade lasers," Opt. Lett. **38**, 1975–1977 (2013).
23. C. Z. Sun, D. Liu, B. Xiong, Y. Luo, J. Wang, Z. B. Hao, Y. J. Han, L. Wang, and H. T. Li, "Modulation characteristics enhancement of monolithically integrated laser diodes under mutual injection locking," IEEE J. Sel. Top. Quantum Electron. **21**, 1802008 (2015).
24. S. T. M. Fryslie, M. P. Tan, D. F. Siriani, M. T. Johnson, and K. D. Choquette, "37-GHz modulation via resonance tuning in single-mode coherent vertical-cavity laser arrays," IEEE Photon. Technol. Lett. **27**, 415–418 (2015).
25. S. T. M. Fryslie, Z. H. Gao, H. Dave, B. J. Thompson, K. Lakomy, S. Y. Lin, P. J. Decker, D. K. McElfresh, J. E. Schutt-Ainé, and K. D. Choquette, "Modulation of coherently coupled phased photonic crystal vertical cavity laser arrays," IEEE J. Sel. Top. Quantum Electron. **23**, 1700409 (2017).
26. Z. X. Xiao, Y. Z. Huang, Y. D. Yang, M. Tang, and J. L. Xiao, "Modulation bandwidth enhancement for coupled twin-square microcavity lasers," Opt. Lett. **42**, 3173–3176 (2017).
27. G. A. Wilson, R. K. DeFreez, and H. G. Winful, "Modulation of phased-array semiconductor lasers at K-band frequencies," IEEE J. Quantum Electron. **27**, 1696–1704 (1991).
28. D. Botez and D. R. Scifres, *Diode Laser Arrays* (Cambridge University, 1994).
29. H. Altug and J. Vučković, "Photonic crystal nanocavity array laser," Opt. Express **13**, 8819–8828 (2005).
30. E. Kapon, J. Katz, and A. Yariv, "Supermode analysis of phase-locked arrays of semiconductor lasers," Opt. Lett. **9**, 125–127 (1984).
31. H. G. Winful and S. S. Wang, "Stability of phase-locking in coupled semiconductor laser arrays," Appl. Phys. Lett. **53**, 1894–1896 (1988).
32. P. Ru, P. K. Jakobsen, J. V. Moloney, and R. A. India, "Generalized coupled-mode model for the multistripe index-guided laser arrays," J. Opt. Soc. Am. B **10**, 507–515 (1993).
33. H. Erzgräber, S. Wieczorek, and B. Krauskopf, "Dynamics of two laterally coupled semiconductor lasers: strong- and weak-coupling theory," Phys. Rev. E **78**, 066201 (2008).
34. Z. Gao, S. T. M. Fryslie, B. J. Thompson, P. Scott Carney, and K. D. Choquette, "Parity-time symmetry in coherently coupled vertical cavity laser arrays," Optica **4**, 323–329 (2017).
35. J. Shena, J. Hizanidis, V. Kovanis, and G. P. Tsironis, "Turbulent chimeras in large semiconductor laser arrays," Sci. Rep. **7**, 42116 (2016).
36. Y. Kominis, V. Kovanis, and T. Bountis, "Controllable asymmetric phase-locked states of the fundamental active photonic dimer," Phys. Rev. A **96**, 043836 (2017).
37. O. Hess and E. Scholl, "Spatio-temporal dynamics in twin-stripe semiconductor lasers," Physica D **70**, 165–177 (1994).
38. N. Blackbeard, H. Erzgräber, and S. Wieczorek, "Shear-induced bifurcations and chaos in models of three coupled lasers," SIAM J. Appl. Dyn. Syst. **10**, 469–509 (2011).
39. S. S. Wang and H. G. Winful, "Dynamics of phase-locked semiconductor laser arrays," Appl. Phys. Lett. **52**, 1774–1776 (1988).
40. H. G. Winful and L. Rahman, "Synchronized chaos and spatiotemporal chaos in arrays of coupled lasers," Phys. Rev. Lett. **65**, 1575–1578 (1990).
41. H. Lamela, M. Leones, G. Carpintero, C. Simmendinger, and O. Hess, "Analysis of the dynamics behavior and short-pulse modulation scheme for laterally coupled diode lasers," IEEE J. Sel. Top. Quantum Electron. **7**, 192–200 (2001).
42. N. Q. Li, H. Susanto, B. R. Cemlyn, I. D. Henning, and M. J. Adams, "Nonlinear dynamics of solitary and optically injected two-element laser arrays with four different waveguide structures: a numerical study," Opt. Express **26**, 4751–4765 (2018).
43. M. J. Adams, N. Q. Li, B. R. Cemlyn, H. Susanto, and I. D. Henning, "Effects of detuning, gain-guiding and index antiguiding on the dynamics of two laterally-coupled semiconductor lasers," Phys. Rev. A **95**, 053869 (2017).
44. R. Santos and H. Lamela, "Experimental observation of chaotic dynamics in two coupled diode lasers through lateral model locking," IEEE J. Quantum Electron. **45**, 1490–1494 (2009).
45. L. Goldberg, H. F. Taylor, J. F. Weller, and D. R. Scifres, "Injection locking of coupledstripe diode laser arrays," Appl. Phys. Lett. **46**, 236–238 (1985).
46. C. M. Long, L. Mutter, B. Dwir, A. Mereuta, A. Caliman, A. Sirbu, V. Iakovlev, and E. Kapon, "Optical injection locking of transverse modes in 1.3-μm wavelength coupled-VCSEL arrays," Opt. Express **22**, 21137–21144 (2014).
47. J. Mercier and M. McCall, "Stability and dynamics of an injection-locked semiconductor laser array," Opt. Commun. **138**, 200–210 (1997).
48. N. Q. Li, H. Susanto, B. R. Cemlyn, I. D. Henning, and M. J. Adams, "Locking bandwidth of two laterally-coupled lasers subjected to optical injection," Sci. Rep. **8**, 109 (2018).
49. N. Q. Li, H. Susanto, B. R. Cemlyn, I. D. Henning, and M. J. Adams, "Injection locking of two laterally-coupled semiconductor laser arrays," Proc. SPIE **10682**, 106820Z (2018).
50. N. Q. Li, H. Susanto, B. R. Cemlyn, I. D. Henning, and M. J. Adams, "Stability and bifurcation analysis of spin-polarized vertical-cavity surface-emitting lasers," Phys. Rev. A **96**, 013840 (2017).